Inversion of Dynamical Scattering from Large-Angle Rocking-Beam Electron Diffraction Patterns

Feng Wang,* Robert S. Pennington, and Christoph T. Koch
Institut für Physik, Humboldt-Universität zu Berlin, Newtonstraße 15, 12489 Berlin, Germany
(Received 24 January 2016; published 30 June 2016)

A method for *ab initio* structure factor retrieval from large-angle rocking-beam electron diffraction data of thin crystals is described and tested with experimental and simulated data. No additional information, such as atomicity or information about chemical composition, has been made use of. Our numerical experiments show that the inversion of dynamical scattering works best, if the beam tilt range is large and the specimen not too thick, because for moderate multiple scattering, the large tilt amplitude effectively removes local minima in this global optimization problem.

DOI: 10.1103/PhysRevLett.117.015501

Electron diffraction, featuring a scattering cross section that is about 5 orders of magnitude larger than that of x-rays or neutrons, is able to probe the atomic structure of crystals only a few nm^3 in size. Crystal structure determination from electron diffraction data has conventionally been an adaptation of kinematic x-ray crystallography methods, such as direct methods [1,2] or the charge flipping algorithm [3]. The success of these techniques for phasing x-ray diffraction patterns of small structures (i.e., proteins up to about 1000 atoms in the asymmetric unit [4]) is based on the fact that with the availability of diffraction data up to a sufficiently high resolution the number of recorded diffraction intensities is much greater than the number of atoms in the structure. However, while in beam-sensitive structures radiation damage makes it often impossible to collect diffraction data up to atomic resolution, dynamical scattering in thicker crystals causes electron diffraction intensities to be a highly nonlinear function of the structure factors, making the kinematic approximation inapplicable in many cases.

Despite these problems, the refinement of crystal structure factors from electron diffraction patterns has a long history [5–8]. Precession electron diffraction (PED) [9] has helped to make electron diffraction data more kinematic-like by averaging over different multiple scattering conditions. Considerable effort has been devoted to matching dynamical diffraction intensities to Bloch wave simulations [10,11], multislice calculations [12–20], or other approaches [21–27].

Convergent beam electron diffraction (CBED) experiments provide two-dimensional rocking curves, i.e., electron diffraction data for a range of slightly different incident beam directions in a single exposure of the diffraction camera. For each of these different incident beam directions the dynamical scattering conditions are slightly different. Matching structure factors to CBED data may thus largely overdetermine the resulting optimization problem, making this technique very sensitive to both amplitude and phase of structure factors.

For conventional CBED patterns, the range of incident beam directions is limited to the first Brillouin zone, since otherwise diffraction discs would overlap. For crystals with lattice parameters smaller than 1 nm, the specimen thickness for quantitative CBED work must thus be rather large (typically 80–150 nm at electron beam energies of 120–200 keV) for the diffraction discs to feature significant changes in the diffraction intensities, making it inapplicable for nanomaterials. In the cases of thin specimens or crystals with lattice parameters much larger than 1 nm, it is very difficult, if not impossible, to obtain CBED patterns with significant variation of intensity within the diffraction discs. By acquiring diffraction data at different beam tilts sequentially, the large-angle rocking-beam electron diffraction (LARBED) technique [28] makes it possible to collect CBED-like 2D rocking curves from nanovolumes for beam tilt angles up to about 100 mrad—i.e., more than 20 times larger than the largest possible convergence angle in CBED experiments of even a small unit cell crystal such as silicon—and this angular range is independent of the size of the unit cell of the diffracting material. While the experimental setup of LARBED is similar to that of PED, the latter is designed to record integrals of ring-shaped rocking curves. The variation of the diffraction intensities with beam tilt is thus lost in PED, but preserved by the LARBED approach. In this Letter, we show that the availability of 2D rocking curve data and the extended range of tilt angles accessible by the LARBED technique in comparison to CBED allows a conventional line search method that minimizes the difference between experimental and simulated LARBED data to determine structure factors in an *ab initio* manner.

Within the Bloch wave scheme, the multiple scattering process of the fast electron traversing a thin crystalline slab is described by the scattering matrix S which, when multiplied by the Fourier representation of the incident wave, sampled at the reciprocal lattice points of the crystal, results in the wave function of the fast electron at the exit face of the specimen,

$$\psi(t,\vec{k}_t,\mathbf{U}_g) = S(t,\vec{k}_t,\mathbf{U}_g)\psi(0), \quad (1)$$

where t is the thickness of the specimen, $\vec{k}_t$ is the transverse component of the wave vector of the incident fast electron relative to the nominal zone axis of the crystal, and $\mathbf{U}_g$ are the complex Fourier coefficients of the electrostatic potential of the crystal being probed by the scattering electrons. $\psi(t,\vec{k}_t,\mathbf{U}_g)$ represents the wave function at the exit surface, and $\psi(0)$ the incident wave. Since $\vec{k}_t$ may also be interpreted as crystal tilt relative to a fixed incident beam direction, $\psi(0)$ does not depend on $\vec{k}_t$. If N_{beams} Bloch states are considered, $S(t,\vec{k}_t,\mathbf{U}_g)$ has $N_{\text{beams}} \times N_{\text{beams}}$ elements, and for an incident plane wave, $\psi(0)$ is a column vector of length N_{beams} with all elements being 0, except for the mth one representing no transverse momentum, the central element in the example below,

$$\psi(0) = [0,0,\ldots,1,\ldots,0,0]^T.$$

With this definition of the incident wave function the intensity measured at reflection $\vec{g}_n$ in the diffraction pattern is given by

$$I_n(t,\vec{k}_t,\mathbf{U}_g) = |\psi(t,\vec{k}_t,\mathbf{U}_g)_n|^2 = |S(t,\vec{k}_t,\mathbf{U}_g)_{n,m}|^2. \quad (2)$$

The scattering matrix can be expressed as

$$S(t,\vec{k}_t,\mathbf{U}_g) = e^{i\pi t A(\vec{k}_t,\mathbf{U}_g)/(\hat{n}\cdot\vec{k})}, \quad (3)$$

where $\vec{k}$ is the wave vector of the incident electron beam corresponding to the electron wavelength $\lambda = 1/|\vec{k}|$. For incident beam directions which are nearly parallel to the surface normal $\hat{n}$ of the crystalline slab this may be approximated as

$$S(t,\vec{k}_t,\mathbf{U}_g) = e^{i\pi\lambda t A(\vec{k}_t,\mathbf{U}_g)}. \quad (4)$$

The structure (Bethe) matrix $A(\vec{k}_t,\mathbf{U}_g)$ at beam tilt $\vec{k}_t$ is

$$A(\vec{k}_t,\mathbf{U}_g) = \begin{pmatrix} \ddots & \vdots & \vdots & \vdots & \vdots & \vdots & \iddots \\ \cdots & -(\vec{k}_t+\vec{h})^2 & \mathbf{U}_{h-g} & \mathbf{U}_h & \mathbf{U}_{h+g} & \mathbf{U}_{h+h} & \cdots \\ \cdots & \mathbf{U}_{g-h} & -(\vec{k}_t+\vec{g})^2 & \mathbf{U}_g & \mathbf{U}_{g+g} & \mathbf{U}_{g+h} & \cdots \\ \cdots & \mathbf{U}_{-h} & \mathbf{U}_{-g} & -\vec{k}_t^2 & \mathbf{U}_g & \mathbf{U}_h & \cdots \\ \cdots & \mathbf{U}_{-g-h} & \mathbf{U}_{-g-g} & \mathbf{U}_{-g} & -(\vec{k}_t-\vec{g})^2 & \mathbf{U}_{-g+h} & \cdots \\ \cdots & \mathbf{U}_{-h-h} & \mathbf{U}_{-h-g} & \mathbf{U}_{-h} & \mathbf{U}_{-h+g} & -(\vec{k}_t-\vec{h})^2 & \cdots \\ \iddots & \vdots & \vdots & \vdots & \vdots & \vdots & \ddots \end{pmatrix},$$

where $\vec{g}$ and $\vec{h}$ are reciprocal-lattice vectors.

The inverse problem we need to solve involves finding all the structure factors $\mathbf{U}_g$ appearing in the matrices $A(\vec{k}_t,\mathbf{U}_g)$ by matching the moduli squared of the entries in the central column of the scattering matrix $S(t,\vec{k}_t,\mathbf{U}_g)$ at known transverse components of the incident wave vector $\vec{k}_t$, to the corresponding measurements, thus optimizing a merit function

$$\chi^2(t,\mathbf{U}_g,\alpha,\beta) = \sum_{l=1}^{N_{\text{tilts}}}\sum_{n=1}^{N_{\text{beams}}}[I_n^{\text{exp}}(\vec{k}_{t_l}) - \alpha|S(t,\vec{k}_{t_l},\mathbf{U}_g)_{n,m}|^2 - \beta]^2, \quad (5)$$

where the thickness t, intensity scale factor α, and intensity offset β are all refined simultaneously.

As every beam tilt requires the computation of the exponential of an $N_{\text{beams}} \times N_{\text{beams}}$ matrix and N_{tilts} may be as large as a few hundreds or even thousands, evaluating the merit function is computationally expensive. Both classic gradient based iterative algorithms as well as heuristic optimization algorithms need to evaluate this function many times. The performance of the optimization algorithm is thus highly influenced by the computational efficiency of the merit function.

A large number of methods for computing the matrix exponential exist [29]. For our dynamical diffraction calculations we use an optimized 9th-order Taylor expansion inside a scaling-and-squaring algorithm implemented for graphics processing units [30], launching multiple matrix exponential calculations in parallel, utilizing dynamic parallelism featured by CUDA version 5 on a workstation containing 3 Nvidia Tesla K20C GPUs and 1 Nvidia Tesla K40C GPU.

To explore the effect that the specimen thickness and tilt range have on the ability of a classical gradient based optimization scheme to determine structure factors *ab initio* from intensity measurements alone, we have applied it to diffraction data simulated for all combinations of the following thicknesses $t = 5$, 10, 20, 40 nm and tilt ranges $\theta_{\text{max}} = \lambda|\vec{k}_t|_{\text{max}} = 5$, 10, 20, 40 mrad. LARBED patterns of $SrTiO_3$ oriented close to the (001) zone axis simulated for these different experimental conditions are shown in Fig. 1. At low specimen thicknesses ($t \leq 10$ nm), the central (undiffracted) disks dominate, implying rather weak scattering and possibly a dominating contribution of kinematical scattering. However, at 10 nm specimen thickness and a tilt range of $|\vec{k}_t|_{\text{max}} = 5$ mrad the complex features in the

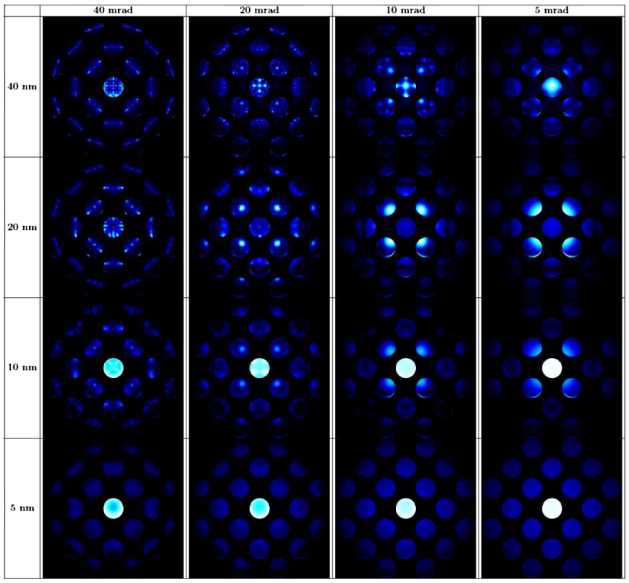

FIG. 1. LARBED patterns of $SrTiO_3$ oriented close to the (001) zone axis simulated for a 120 keV electron beam, with 45 beams selected. Within the discs of radius $\theta_{\max} = 5$, 10, 20, and 40 mrad, 1024 different beam tilt vectors uniformly distributed within these discs have been chosen. The different rows represent specimen thicknesses of 5, 10, 20, and 40 nm.

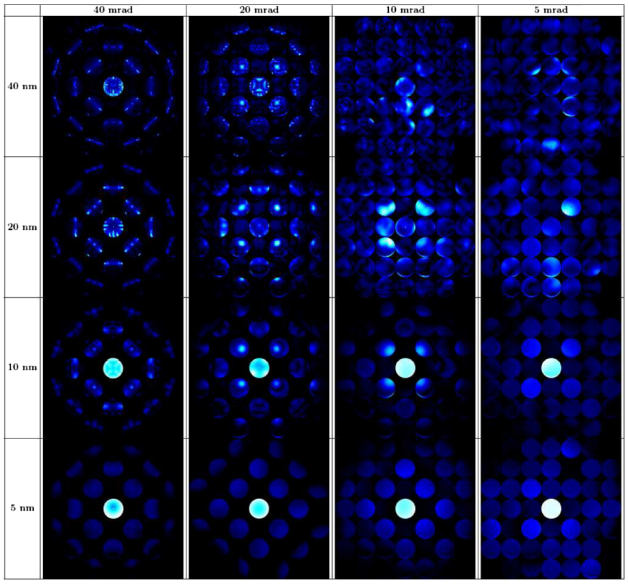

FIG. 2. LARBED patterns simulated from the structure factor fitted to the simulated data shown in Fig. 1 by minimizing expression (5).

diffracted discs indicate that the dynamical contribution to the observed intensities is already very significant. At higher specimen thicknesses the intensity of the undiffracted beam is already lower than that of some reflections, at least at the zone axis.

The diffraction patterns shown in Fig. 1 each show 21 strong diffraction discs. However, in addition to the visible discs, the very weak reflections between them (100, 210, etc.) have been included in the calculation as well, resulting in a structure factor matrix $A(\vec{k}_t, \mathbf{U}_g)$ of size 45×45, i.e., with $N_{\text{beams}} = 45$, containing 157 unique structure factors, since this matrix also contains structure factors corresponding to the difference of any pair of computed reflections. For the structure factor determination, all structure factors were initialized to $\mathbf{U}_g = (0.01 + 0.01i)$ Å^{-2} and the thickness was initialized to the value for which each of the patterns was simulated. At large specimen thicknesses and small tilt range (as in the case of CBED), the optimization routine tended to get stuck in local minima. But even for thin specimens, the tilt amplitudes must be large for the optimization to be successful, i.e., for a final R value of $\leq 10\%$, where

$$R(t,\mathbf{U}_g,\alpha,\beta) = \frac{\sum_{l=1}^{N_{\text{tilts}}}\sum_{n=1}^{N_{\text{beams}}} \left|\sqrt{I_n^{\text{exp}}(\vec{k}_{t_l})} - \alpha\sqrt{|S(t,\mathbf{U}_g,\vec{k}_{t_l})_{n,m}|^2} - \beta\right|}{\sum_{l=1}^{N_{\text{tilts}}}\sum_{n=1}^{N_{\text{beams}}}\sqrt{I_n^{\text{exp}}(\vec{k}_{t_l})}}. \quad (6)$$

To confirm our interpretation of the R value, Fig. 2 shows the diffraction patterns that have been simulated from the set of recovered structure factors and specimen thicknesses. For the patterns with smaller tilt amplitudes, especially for the $\theta_{\max} = 5$ mrad case, all the very weak reflections with index sums $h + k + l =$ odd in Fig. 1 appear rather strong, indicating a very poor fit because the optimization algorithm got stuck in a local optimum. Only for the largest tilt range of 40 mrad, all the fitted patterns for thicknesses up to 20 nm show good agreement with the simulated data. At a thickness of 40 nm the intensity distribution within the diffraction discs does not really correspond to the original. This is obvious again when looking at the very weak reflections.

From the structure factor amplitudes and phases, we also computed the projected unit cell potential by inverse Fourier transform (see Fig. 3). Since the structure factor matrix has not been constrained for symmetry nor for Hermiticity during the refinement, the projected potential is complex valued, with the real part describing pure elastic scattering, and the imaginary part absorption. The appearance of the weak oxygen columns in the potential maps may be used as an indicator of how well the structure factors have been determined. Comparing the reconstructed potential maps with the one corresponding to the structure factors used to simulate the LARBED patterns, it is obvious that only for the largest beam tilt ranges and moderate thicknesses, the optimization routine has successfully converged at least close to the global optimum, i.e., could determine 157 $\mathbf{U}_g$ from LARBED discs of 45 "measured" reflections.

To further quantify the ability of our approach to determine the correct structure factor phases, three-phase invariant errors have been computed. The sum of the phases of three structure factors corresponding to lattice vectors

that form a closed loop, i.e., $\phi_{g,h} = \phi_g + \phi_h + \phi_{-g-h}$, is independent of the choice of unit cell origin and thus a well-defined quantity. We have thus evaluated the following three-phase invariant error

$$E_{\text{triplet}} = \frac{\sum_{g,h} |\phi_{g,h} - \phi_{\text{theory}}| \sqrt[3]{|\mathbf{U}_g \mathbf{U}_h \mathbf{U}_{-g-h}|}}{\sum_{g,h} \sqrt[3]{|\mathbf{U}_g \mathbf{U}_h \mathbf{U}_{-g-h}|}},$$

averaging over all possible structure factor phase triplets that can be constructed from the 45 structure factors of the measured reflections. Here, ϕ_{theory} is the theoretical phase invariant, and for centrosymmetric $SrTiO_3$, this value is either 0 or π. For each of the test cases the corresponding value of E_{triplet} is shown in Fig. 3. The errors for the patterns with larger tilt amplitudes are generally smaller than for patterns with smaller tilt amplitudes. Setting a threshold of 0.3, we can say that reconstructed structure factor sets with a mean phase triplet error below this value correspond to a potential map which agrees reasonably with the original one, at least when not considering very high-order reflections, diffraction intensities of which have not been measured.

Figure 4(a) shows experimental LARBED data of $SrTiO_3$ oriented near the (001) zone axis, captured automatically by the QED software (HREM Research Inc., Higashimastuyama, Japan) on a Gatan Orius 200W CCD camera installed on a Zeiss EM912 operated at an accelerating voltage of 120 kV. Although this microscope is equipped with an in-column energy filter, these data have not been zero-loss filtered in order to show the robustness of our structure factor determination scheme against unfavorable experimental conditions, making it easily comparable with conventional electron diffraction experiments. The LARBED data set consists of 1009 diffraction patterns acquired at beam tilts which fill a disc of radius $\theta_{\text{max}} = 70$ mrad. Integrated background-substracted intensities of 121 diffraction spots have been extracted from each of the experimental diffraction patterns. Since no energy filtering was applied, and the expected localization of much of the inelastic scattering occurs at small scattering angles, we have omitted the undiffracted and the first order reflections from the fit, i.e., reflections 000, 100, 010, $\bar{1}00$, and $0\bar{1}0$.

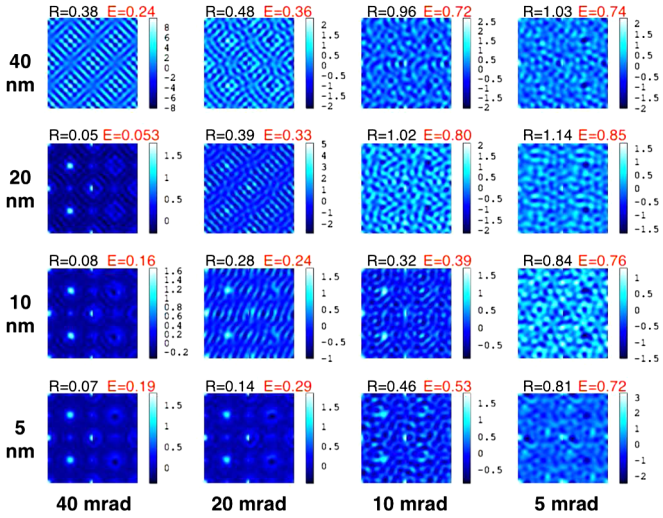

FIG. 3. Maps of the projected potential of 2×2 unit cells corresponding to the recovered sets of structure factors. The reconstructed potential maps are shown on the left-hand side, the differences between the reconstructed and the theoretical maps are shown on the right-hand side. The numbers in the top right corner of each of these maps represent E_{triplet}, i.e., the mean of 1189 phase triplet errors computed from those $\mathbf{U}_g$ for which intensity measurements have been included in the optimization, i.e., which appear in the mth column of the structure factor matrix. The numbers in the top left corner of each map indicate the R value calculated from Eq. (6).

Adding a $|\mathbf{U}_g|$ penalty term to the absolute-value norm of the intensity differences, we minimized a modified target function

$$E(t, \mathbf{U}_g, \alpha, \beta) = \sum_{l=1}^{N_{\text{tilts}}} \sum_{n=1}^{N_{\text{beams}}} |I_n^{\text{exp}}(\vec{k}_{t_l}) - \alpha |S(t, \mathbf{U}_g, \vec{k}_{t_l})_{n,m}|^2 - \beta| + \gamma \sum_g |\mathbf{U}_g|^2,$$

where $\gamma = N_{\text{tilt}}/10$. This additional penalty term is designed to prevent the structure factors of some unmeasured reflections to become exceedingly large. From this experimental LARBED data for 121 reflections we have successfully determined 456 structure factors $\mathbf{U}_g$, the specimen thickness, and other parameters related to the experiment, such as a refinement of the beam tilts. The best fitting LARBED pattern [Fig. 4(b)] was obtained for a specimen thickness of 11.5 nm. The corresponding potential map is shown in Fig. 4(e). The rather large values in the imaginary part of the potential are likely due to the fact that the experimental data had not been zero-loss filtered. Figure 4(f) shows the map of the projected potential obtained from all 456 structure factors that have been fitted to the experimental data, but including a term in which penalizes differences in $|\mathbf{U}_g|$ for reflections that have very similar integrated intensities, i.e., for which a kinematic fit to the data would yield nearly identical structure factor amplitudes. Including a larger number of structure factors yields much sharper peaks at the positions of the atomic columns, as would be expected.

We have investigated the feasibility of *ab initio* structure factor determination from both simulated and experimental LARBED intensities alone. We avoided applying any additional constraints to the structure factors, such as symmetry or atomicity, in order to demonstrate the applicability of this approach also in cases where radiation damage prevents the acquisition of diffraction data up to atomic resolution.

We were able to determine 456 structure factors from experimental LARBED data of 11.5 nm thick $SrTiO_3$, even though only 121 diffraction spots have been included in the analysis. All atomic columns, including those containing

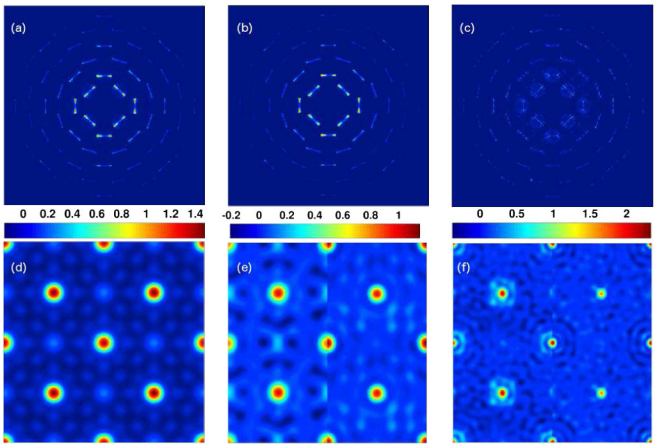

FIG. 4. (a) Experimental LARBED pattern of $SrTiO_3$ comprising 1009 different beam tilts. (b) LARBED pattern simulated from the set of reconstructed structure factors, assuming no additional information about the specimen other than the experimental data. (c) Difference of the intensities shown in (a) and (b). (d) Theoretical map of the (001)-projected potential of $SrTiO_3$ as represented by the first 121 reflections in this orientation. The projected potential of 2×2 unit cells is shown [same in (e) and (f)]. (e) Reconstructed potential map corresponding to the first 121 beams, applying no additional (symmetry) constraints. The real part of the projected potential is shown on the left-hand side, and the imaginary part on the right-hand side [same in (f)]. (f) Reconstructed potential map with all 456 different structure factors, but constraining some $|\mathbf{U}_g|$'s as explained in the text.

only oxygen, have been recovered. Testing our approach on simulated data we find that for a small range of beam tilts, such as in the case of conventional CBED, the optimization routine was not able to get close to the global optimum. This is due to a lack of features across the disks when the specimen is thin, and too much multiple scattering when the specimen is thicker. To retrieve the structure factor phases reliably by this approach there must be a moderate multiple scattering, and the range of incident beam tilts must be several times larger than that accessible in conventional CBED experiments.

The source code of the structure factor refinement program, written in C++, is available at github [31].

The authors acknowledge funding by the Carl Zeiss Foundation as well as the German Research Foundation (Grants No. KO 2911/7-1 and SFB 951).

*feng.wang@physik.hu-berlin.de

[1] J. Karle, in *Nobel Lectures, Chemistry 1981–1990*, edited by T. Frängsmyr and B. G. Malmström (World Scientific, Singapore, 1992), p. 218.
[2] H. Hauptman, in *Nobel Lectures, Chemistry 1981–1990*, edited by T. Frängsmyr and B. G. Malmström (World Scientific, Singapore, 1992), p. 186.
[3] G. Oszlanyi and A. Suto, Acta Crystallogr. Sect. A **60**, 134 (2004).
[4] H. Hauptman, Curr. Opin. Struct. Biol. **7**, 672 (1997).
[5] J. M. Cowley, *Diffraction Physics*, 3rd ed., North-Holland personal library (Elsevier Science B.V, New York, 1995).
[6] B. K. Vainshtein, *Structure Analysis by Electron Diffraction* (Elsevier, New York, 2013).
[7] T. E. Weirich, J. L. Lábár, and X. Zou, *Electron Crystallography: Novel Approaches for Structure Determination of Nanosized Materials* (Springer Science & Business Media, 2006), Vol. 211.
[8] D. L. Dorset, *Structural Electron Crystallography* (Springer Science & Business Media, New York, 2013).
[9] R. Vincent and P. A. Midgley, Ultramicroscopy **53**, 271 (1994).
[10] J. C. H. Spence and J. M. Zuo, *Electron Microdiffraction* (Springer, Boston, MA, 1992).
[11] L. Palatinus, D. Jacob, P. Cuvillier, M. Klementova, W. Sinkler, and L. D. Marks, Acta Crystallogr. Sect. A **69**, 171 (2013).
[12] J. C. H. Spence, Acta Crystallogr. Sect. A **49**, 231 (1993).
[13] J. C. H. Spence, Acta Crystallogr. Sect. A **54**, 7 (1998).
[14] J. C. H. Spence, B. Calef, and J. M. Zuo, Acta Crystallogr. Sect. A **55**, 112 (1999).
[15] L. J. Allen, T. W. Josefsson, and H. Leeb, Acta Crystallogr. Sect. A **54**, 388 (1998).
[16] L. J. Allen, H. Leeb, and A. E. C. Spargo, Acta Crystallogr. Sect. A **55**, 105 (1999).
[17] L. J. Allen, H. M. L. Faulkner, and H. Leeb, Acta Crystallogr. Sect. A **56**, 119 (2000).
[18] L. J. Allen, C. Koch, M. P. Oxley, and J. C. H. Spence, Acta Crystallogr. Sect. A **57**, 473 (2001).
[19] J. M. Zuo and J. C. H. Spence, Ultramicroscopy **35**, 185 (1991).
[20] J. M. Zuo and J. L. Rouviére, IUCrJ **2**, 7 (2015).
[21] H. W. Zandbergen, Science **277**, 1221 (1997).
[22] J. Jansen, D. Tang, H. W. Zandbergen, and H. Schenk, Acta Crystallogr. Sect. A **54**, 91 (1998).
[23] J. Friis, B. Jiang, J. Spence, K. Marthinsen, and R. Holmestad, Acta Crystallogr. Sect. A **60**, 402 (2004).
[24] L. N. Bakken, K. Marthinsen, R. Hier, and R. Holmestad, Micron and microscopica acta **23**, 137 (1992).
[25] D. M. Bird and M. Saunders, Acta Crystallogr. Sect. A **48**, 555 (1992).
[26] T. E. Weirich, R. Ramlau, A. Simon, S. Hovmöller, and X. Zou, Nature (London) **382**, 144 (1996).
[27] R. Imlau, A. Kovcs, E. Mehmedovic, P. Xu, A. A. Stewart, C. Leidinger, R. E. Dunin-Borkowski, G. Bihlmayer, H. Wiggers, R. Carius, U. Kolb, and M. Luysberg, Phys. Rev. B **89**, 054104 (2014).
[28] C. T. Koch, Ultramicroscopy **111**, 828 (2011).
[29] C. Moler and C. Van Loan, SIAM Rev. **20**, 801 (1978).
[30] R. S. Pennington, F. Wang, and C. T. Koch, Ultramicroscopy **141**, 32 (2014).
[31] https://github.com/fengwang/larbed-refinement.